

# Nanoscale

Accepted Manuscript



This is an *Accepted Manuscript*, which has been through the Royal Society of Chemistry peer review process and has been accepted for publication.

*Accepted Manuscripts* are published online shortly after acceptance, before technical editing, formatting and proof reading. Using this free service, authors can make their results available to the community, in citable form, before we publish the edited article. We will replace this *Accepted Manuscript* with the edited and formatted *Advance Article* as soon as it is available.

You can find more information about *Accepted Manuscripts* in the [Information for Authors](#).

Please note that technical editing may introduce minor changes to the text and/or graphics, which may alter content. The journal's standard [Terms & Conditions](#) and the [Ethical guidelines](#) still apply. In no event shall the Royal Society of Chemistry be held responsible for any errors or omissions in this *Accepted Manuscript* or any consequences arising from the use of any information it contains.

## ARTICLE

# Growth of metal-catalyst-free nitrogen-doped metallic single-wall carbon nanotubes

Cite this: DOI: 10.1039/x0xx00000x

Jin-Cheng Li<sup>§</sup>, Peng-Xiang Hou<sup>§</sup>, Lili Zhang, Chang Liu,\* Hui-Ming Cheng

Received 00th January 2014,  
Accepted 00th January 2014

DOI: 10.1039/x0xx00000x

[www.rsc.org/](http://www.rsc.org/)

Nitrogen-doped (N-doped) single-wall carbon nanotubes (SWCNTs) were synthesized by chemical vapor deposition using SiO<sub>x</sub> nanoparticles as catalyst and ethylenediamine as the source of both carbon and nitrogen. The N-doped SWCNTs have a mean diameter of 1.1 nm and a narrow diameter range, with 92% having diameters from 0.7 to 1.4 nm. Multi-wavelength laser Raman spectra and temperature-dependent electrical resistance indicate that the SWCNT sample is enriched with metallic nanotubes. These N-doped SWCNTs showed excellent electrocatalytic activity for the oxygen reduction reaction and highly selective and sensitive sensing ability for dopamine detection.

## Introduction

Single-wall carbon nanotubes (SWCNTs) have a wide-range of potential applications in electronic devices, sensors, composites, energy storage devices, catalysis systems, etc.,<sup>1-9</sup> due to their extraordinary physical and chemical properties. A SWCNT can be either semiconducting or metallic depending on its chirality. Semiconducting SWCNTs (s-SWCNTs) and metallic-SWCNTs (m-SWCNTs) are respectively considered to be an ideal channel material and interconnector in high-performance electronic devices. However, as-grown SWCNT samples are usually a mixture of s- and

m-SWCNTs. Therefore, selective growth of pure s-SWCNTs and m-SWCNTs is of great importance.

In recent years, notable progress has been made on the direct growth of s-SWCNTs, by either catalyst engineering or selective etching.<sup>10-15</sup> However, because m-SWCNTs are chemically more active than s-SWCNTs, the selective growth of m-SWCNTs is even more challenging.<sup>16</sup> Heteroatom doping with elements such as nitrogen and boron, has been regarded an effective pathway to tailor the electronic properties of SWCNTs. Li et al.<sup>17</sup> reported that surface-grown N-doped SWCNTs behave like metallic nanotubes.

Maruyama et al.<sup>18</sup> reported that nitrogen-doping reduced the diameter of vertically aligned SWCNTs, while Kauppinen et al.<sup>19-21</sup> claimed that the introduction of NH<sub>3</sub> during the chemical vapor deposition (CVD) synthesis process led to the preferential growth of large-diameter s-SWCNTs with large chiral angles. Recently, Wagberg et al.<sup>22</sup> reported that the incorporation of nitrogen narrows the chirality distribution of SWCNTs. These results about N-doped SWCNTs are not consistent, and how nitrogen influences the diameter and conductivity of SWCNTs is unclear. In addition, all previous studies used metal catalysts for the growth of nitrogen-doped SWCNTs, and the residual metal impurity may degrade their properties and hinder their application in electronic and bio-devices.

In this study we synthesize metal-free N-doped SWCNTs by a CVD method using SiO<sub>x</sub> as catalyst and ethylenediamine as both carbon and nitrogen source. Compared with un-doped SWCNTs, the N-doped SWCNTs show a much narrower diameter distribution with a mean diameter of 1.1 nm with 92% of the nanotubes having diameters ranging from 0.7 to 1.4 nm. Laser Raman spectroscopy and surface resistance measurements show that the N-doped SWCNT sample is enriched with metallic nanotubes. The possible mechanism for the influence of nitrogen-doping on the structure and conductivity of SWCNTs is discussed. In addition, these N-doped m-SWCNTs show excellent electrocatalytic activity for the oxygen reduction reaction and sensing ability for dopamine detection when used as electrodes.

## Experimental methods

### 1. Preparation of SiO<sub>x</sub> catalyst

The detailed preparation of the SiO<sub>x</sub> catalyst was given in our previous report.<sup>23, 24</sup> Typically, a 30 nm-thick SiO<sub>x</sub> film was deposited on a Si/SiO<sub>2</sub> wafer (Si wafer with a 300-nm-thick thermally-grown oxide layer) by ion-beam sputtering at a deposition

rate of 0.04-0.05 nm/s. The Si/SiO<sub>2</sub> film was then annealed at 900 °C for 10 min under a mixed Ar (200 standard cubic centimeter per minute (sccm)) and H<sub>2</sub> (50 sccm) flow.

### 2. Synthesis of N-doped and un-doped SWCNTs

For the growth of N-doped SWCNTs, the Ar (200 sccm) was bubbled through an ethylenediamine solution kept at 40 °C using a water bath. The growth time was 10 min. The bubbling of ethylenediamine was then terminated, and the grown sample was rapidly pushed into a low temperature zone. For the growth of un-doped SWCNTs, identical growth conditions were used, but ethanol was substituted for ethylenediamine as a carbon source.

### 3. Characterization of the SWCNTs

The SWCNT samples were characterized by scanning electron microscopy (SEM, Nova NanoSEM 430, operated at 15kV), Raman spectroscopy (JobinYvonHR800, excited by a laser with a spot size of ~1 μm<sup>2</sup>), X-ray photoelectron spectroscopy (XPS, Escalab 250, Al K<sub>α</sub>) and transmission electron microscopy (TEM, TecnaiF20, 200 kV).

For resonance Raman measurements, three laser wavelengths of 532, 633 and 785 nm were used. A 100× objective lens was used to focus the laser beam. Line sweep over 50 different spots on each sample and laser wavelength was performed, and the distance between adjacent points was 5-10 μm.

For TEM observations, we used a flexible poly (methyl-methacrylate) (PMMA) film to transfer SWCNTs from the original substrate to a Cu TEM grid. A PMMA solution (AR-P 679, 4 wt.% ethyl lactate, Allresist) was first spin-coated (3000 rpm for 1 min) on the substrate on which the SWCNTs were grown, and then baked at 60 °C for 30 min in air. The substrate was then coated with a PMMA film and put into a 5 M NaOH aqueous solution kept at 60 °C for 2 h. The PMMA film with embedded SWCNTs was peeled off and

## Journal Name

attached onto a Cu grid, after which the PMMA was removed by a hot acetone bath.

Temperature-dependent electrical resistance measurements were performed using a four-point probe method. The testing temperature range was 295 to 20 K.

#### 4. Measurements of oxygen reduction reaction (ORR) and electrochemical sensing performance

Cyclic voltammetric (CV) measurements were performed using a program-controlled potentiostat (CHI 730 C) in a standard three-electrode cell. A SWCNT electrode was used as the working electrode and a Pt wire served as the counter electrode. For ORR measurements, an aqueous solution of KOH (0.1 M) was used as electrolyte, and an Ag/AgCl electrode (filled with 10% KNO<sub>3</sub> solution) as reference electrode. N<sub>2</sub> or O<sub>2</sub> was used to purge the solution to obtain oxygen-free or oxygen-saturated electrolyte solutions. The test was performed at a scan rate of 100 mV/s. The working electrode was prepared using a Nafion solution (5%) to transfer SWCNTs from a silicon wafer to a glassy carbon (GC) electrode. Measurement on a rotating disk electrode was carried out on a modulated speed electrode rotator (Pine Instrument). For a quantitative evaluation of the ORR electrocatalytic activity, rotation-rate-dependent rotating disk electrode (RDE) measurements were performed based on the Koutecky-Leviche equation.<sup>25</sup>

For the electrochemical dopamine (DA) and ascorbic acid (AA) sensing measurements, a 0.025 M phosphate buffer solution (PBS, PH 6.9) saturated with Ar was used as the electrolyte and an Ag/AgCl served as the reference electrode. The scan rate was 50 mV/s. The electrode preparation was similar to that described above.

## Results and Discussion

Figure 1 shows typical (a, b) SEM and (c, d) TEM images of the as-synthesized (a, c) N-doped and (b, d) un-doped SWCNTs. From SEM observations, we can see that a dense and clean SWCNT network was obtained in both cases, but the N-doped SWCNTs are usually more bent. TEM images show that the diameters of the N-doped SWCNTs (Figure 1c) are smaller than those of the un-doped SWCNTs (Figure 1d). The diameters of 259 N-doped and 212 un-doped SWCNTs were measured under TEM, and the resultant diameter distributions of these two samples are shown in Figures 1e and f. It can be seen that the mean diameter of the N-doped SWCNTs is 1.1 nm, much smaller than the 1.6 nm for the un-doped SWCNTs. Furthermore, the diameter distribution of the N-doped SWCNTs is much narrower than that of the un-doped SWCNTs. 92% of the N-doped SWCNTs have diameters ranging from 0.7 to 1.4 nm. This result suggests that the presence of nitrogen during the CVD process significantly affects the diameter of the SWCNTs produced.

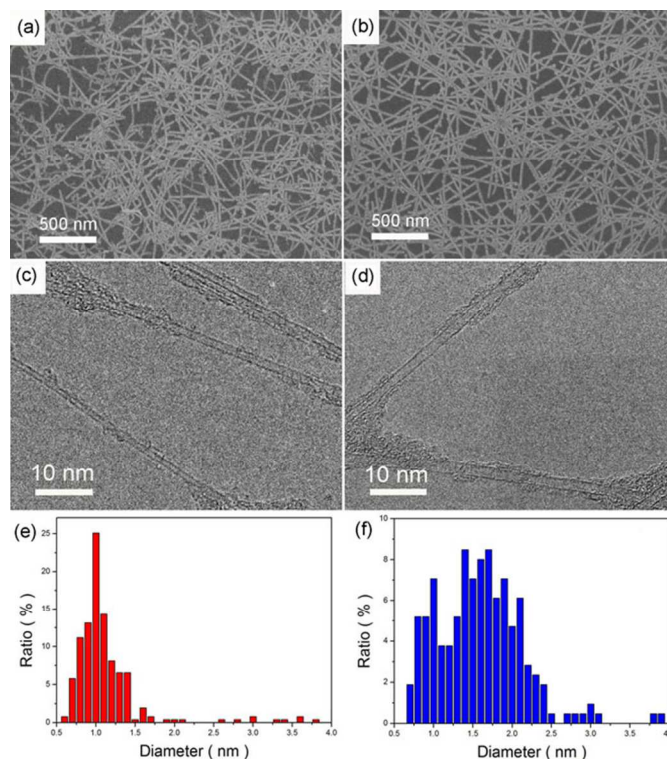


Figure 1. Typical (a, b) SEM, (c, d) TEM images, and (e, f) diameter

distributions of the N-doped (a, c, e) and un-doped (b, d, f) SWCNTs.

The N-doped and un-doped SWCNTs were further characterized using laser Raman spectroscopy with excitation laser wavelengths of 532, 633 and 785 nm. Figure 2 shows the typical radial breathing mode (RBM) peaks obtained from 532 and 633 nm lasers. Intense RBM peaks are clearly resolved for both samples, confirming that the samples are composed of SWCNTs. We estimated the diameter of the SWCNTs using an empirical relation:  $d_{\text{SWCNT}} = \frac{248}{\omega_{\text{RBM}}}$ , where

$\omega_{\text{RBM}}$  is the Raman shift in  $\text{cm}^{-1}$  and  $d_{\text{SWCNT}}$  is the tube diameter in nm. The diameter distributions of the N-doped and un-doped SWCNTs were calculated to be in the range of 0.7-1.4 nm and 0.7-2.5 nm, respectively, agreeing well with the results of TEM observations. According to the Kataura plot, the RBM peaks can be assigned to metallic or semiconducting SWCNTs, based on the Raman shift and excitation laser wavelength.<sup>26</sup> As can be seen in Figure 2c-d, both metallic and semiconducting SWCNTs exist in the un-doped sample. However, in Figures 2a and 2b, the majority of the RBM peaks originate from metallic tubes for the N-doped SWCNT sample. In the Raman spectra excited by 785 nm laser (Figure S1), small-diameter s-SWCNT peaks were detected, but the intensities of these peaks were very weak suggesting few s-SWCNTs existed in the sample. These results indicate that the growth of m-SWCNTs with diameters of 1.2-1.4 nm is apparently enhanced when nitrogen is introduced, i.e. nitrogen may significantly influence both the diameter and conductivity of SWCNTs.

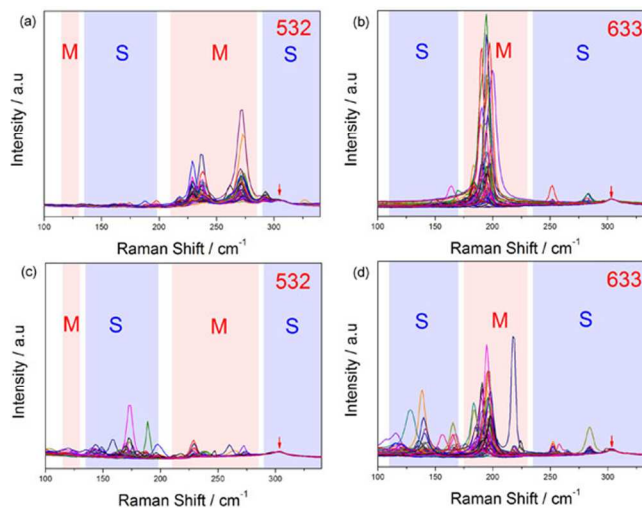


Figure 2. Raman spectra of (a, b) the N-doped and (c, d) un-doped SWCNTs excited by 532 (a, c) and 633 (b, d) nm lasers. The regions corresponding to semiconducting and the metallic transitions are labeled as S (cyan zone) and M (magenta zone). Each spectrum is normalized with respect to the  $303 \text{ cm}^{-1}$  peak (red arrow) from the Si/SiO<sub>2</sub> substrate.

The high phonon frequencies (D band, G band and 2D band) of Raman spectroscopy are very sensitive to the structure of SWCNTs. As shown in Figure 3a, the intensity ratio of the G band to the D band ( $I_G/I_D$ ) decreased from 33.6 for the un-doped SWCNTs to 17.7 for the N-doped SWCNTs. This is because, when nitrogen is incorporated into the SWCNTs, defects are introduced and consequently the intensity of the D band increases. In addition, the larger curvature of the thinner N-doped SWCNTs results in greater lattice deformation of the tube walls. It is well known that the second order phonon frequencies are highly sensitive to a change in the  $\text{sp}^2$  carbon structure. Comparing the N-doped SWCNTs with un-doped SWCNTs, we can see that the D band and 2D band are red shifted while the G band is slightly blue shifted, which is strong evidence of nitrogen incorporation into the structure of the SWCNTs. The G band of the N-doped SWCNTs is divided distinctly into G<sup>-</sup> (1545-1558  $\text{cm}^{-1}$ ) and G<sup>+</sup> (1597  $\text{cm}^{-1}$ ) peaks (Figure 3a). The diameter of

SWCNTs can be calculated from:  $\omega_{G^+} - \omega_{G^-} = \frac{c}{(d_{SWCNT})^2}$ <sup>27</sup>,

where *c* is a constant, depending on whether the SWCNTs are metallic (*c*=79.5) or semiconducting (*c*=47.7). As discussed above, the diameters of our N-doped SWCNTs are mainly in the range of 1.2-1.4 nm. Taking a mean tube diameter of 1.3 nm and a G<sup>+</sup> peak position of 1552 cm<sup>-1</sup>, the *c* value is calculated to be ~76.0, which further confirms that our N-doped SWCNTs are enriched with metallic nanotubes.

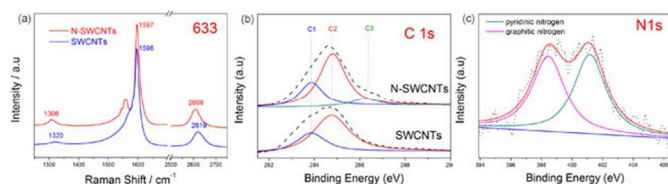


Figure 3. (a) D band, G band and 2D band Raman spectra of the N-doped (upper) and un-doped (lower) SWCNTs excited by a 633 nm laser. (b) C 1s spectra of the N-doped and un-doped SWCNTs. (c) Typical N 1s spectrum of the N-doped SWCNTs.

We further quantitatively examined the form and content of nitrogen incorporated in the N-doped SWCNTs using XPS measurements. Compared with the un-doped SWCNTs, an additional C1s peak appears at 286.3 eV for the N-doped sample (C3, Figure 3b). This peak is assigned to a C-N bond,<sup>28</sup> indicating that nitrogen has been incorporated into the framework of the SWCNTs. The N1s spectrum of the N-doped SWCNT sample is shown in Figure 3c, and can be fitted into two peaks centered at 398.5 eV and 401.2 eV, corresponding to pyridinic nitrogen (50.8 at.%) and graphitic nitrogen (49.2 at.%), respectively. The nitrogen content calculated from the area ratio of N1s to C1s signals corrected with standard XPS sensitivity factors is 4.0 at.%.

Based on the above results, N-doped SWCNTs with a smaller mean diameter and narrower diameter distribution compared with un-doped SWCNTs were synthesized under identical conditions

(except for the feedstock). This phenomenon can be understood from the change of SWCNT growth mode from tangential growth to perpendicular growth owing to the action of nitrogen on catalyst particles proposed by Maruyama group<sup>29</sup>. Our TEM observations also verify the above proposition as shown in Figure S2. In Figure S2a we can see that an un-doped SWCNT grows from a catalyst nanoparticle in a tangential mode, i.e. the tube wall is tangential to the spherical particle. As a result, the diameter of the SWCNTs is roughly the same as that of the catalyst nanoparticle. However, for the N-doped SWCNTs we can see that the nanotube grows in a perpendicular manner (Figure S2b), i.e. the tube wall is perpendicular to the outer surface of the catalyst nanoparticle. In this case, the diameter of the N-doped SWCNT is smaller than that of the catalyst particle. Figure S2c schematically shows the growth of N-doped and un-doped SWCNTs from catalyst nanoparticles.

It is well known that the introduction of nitrogen into the framework of SWCNTs changes their electron-density distribution. Pyridinic nitrogen (p-type doping)/graphitic nitrogen (n-type doping) will down-shift/up-shift the Fermi level closer to the valence band/conduction band, which results in an improvement of electrical conductivity.<sup>30, 31</sup> Maniwa et al.<sup>32</sup> reported that low temperature four-point electrical resistance measurements can be used to analyze the content of s-SWCNTs and m-SWCNTs due to the completely different transport mechanisms of their networks. We measured the electrical resistance of the N-doped and un-doped SWCNT networks in the temperature range 20–295 K. As can be seen in Figure 4a, totally different curve types are obtained for these two samples. The resistance of the un-doped SWCNTs has a rough exponential relationship with temperature, while the resistance of the N-doped SWCNTs remains almost unchanged in the temperature range examined. The values of  $R(20\text{ K})/R(295\text{ K})$  for the N-doped and un-doped SWCNTs are 1.16 and 5.20, respectively. These results

indicate that the N-doped SWCNT is metallic, while the un-doped SWCNT sample is a mixture of metallic and semiconducting nanotubes.<sup>32</sup> Therefore, both multi-wavelength laser Raman spectroscopy and resistance measurements at different temperatures show that m-SWCNTs are obtained when nitrogen is introduced. On the one hand, the metallic behavior of the N-doped SWCNTs can be ascribed to the incorporation of nitrogen into the graphitic structure of SWCNTs.<sup>31</sup> On the other hand, nitrogen doping may also exert an influence on the carbon/catalyst interaction and SWCNT nucleation,<sup>7</sup> which leads to the formation of small diameter SWCNTs with more metallic character (as characterized by laser Raman spectroscopy).

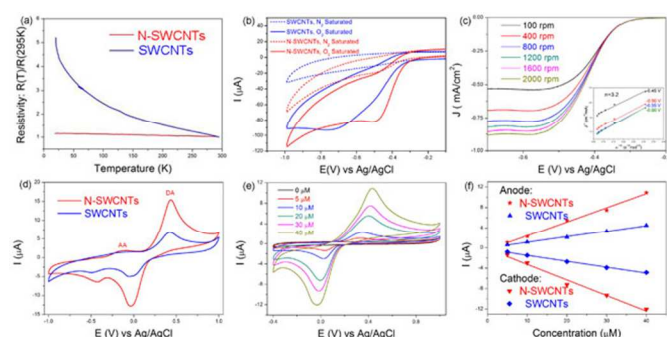


Figure 4 (a) Temperature dependence of surface resistivity of the N-doped and un-doped SWCNTs. (b) CVs at a scan rate of 100 mV/s in 0.1 M KOH solution saturated with O<sub>2</sub> (solid line) and N<sub>2</sub> (dashed line) for the N-doped and un-doped SWCNTs. (c) RDE linear sweep curves of the N-doped SWCNTs in an oxygen-saturated 0.1 M KOH solution with different speeds at a scan rate of 5 mV/s (the inset shows the Koutecky-Levich plots of the N-doped SWCNTs derived from RDE measurements). (d) CVs of the N-doped and un-doped SWCNTs in a PBS solution containing 40 μM DA and 40 μM AA. (e) CVs of the N-doped SWCNTs in PBS solutions containing 0, 5, 10, 20, 30, and 40 μM DA saturated with Ar. (f) Plots of anodic and cathodic peak currents of the N-doped and un-doped SWCNTs as a function of DA concentration.

It was reported that N-doped SWCNTs showed high electrocatalytic activity for the ORR<sup>33</sup> and could replace Pt-based

electrocatalyst in fuel cells. As discussed above, we prepared N-doped SWCNTs with small diameters, high nitrogen content and a metallic transport feature. Such a material may have superior electrocatalytic activity. Therefore, the as-prepared N-doped SWCNTs were used as an electrode for ORR. For comparison, the performance of the un-doped SWCNTs was also tested. As shown in Figure 4b, the N-doped SWCNT/GC electrode shows a substantial reduction process at about -0.50 V in the presence of O<sub>2</sub>, while a much weaker response was observed at the same potential under N<sub>2</sub> atmosphere, indicating that the N-doped SWCNTs have electrochemical activity for ORR. As for the un-doped SWCNTs, the reduction potential decreased by 0.23 V and the onset potential shifted to a more negative value compared with the N-doped SWCNTs. This result indicates that nitrogen-doping increases the ORR electrocatalytic activity of SWCNTs, consistent with the previous report.<sup>17</sup> In addition, we used the Koutecky-Levich equation to determine the transferred electron number per oxygen molecule involved into the ORR process of N-doped SWCNTs (details see supporting information (SI)). ORR polarization curves of the un-doped and N-doped SWCNTs at 1600 rpm shows a two-step (2e<sup>-</sup> process) and a one-step (4e<sup>-</sup>) wide platform, respectively (Figure S3). The number of transferred electrons per oxygen molecule was calculated to be mean 3.2 in the potential range of -0.45 to -0.6 V in Figure 4c (inset), suggesting that a four-electron pathway is the main reaction process with H<sub>2</sub>O as product, which is consistent with previous reports.<sup>33, 34</sup>

SWCNTs are an ideal candidate for chemical sensors due to their high surface area, large aspect ratio,<sup>35</sup> good stability, and outstanding ability to mediate fast electron-transfer kinetics for important biomolecules,<sup>9, 36</sup> such as DA and AA. DA and AA coexist in the extra cellular fluid of the central nervous system and serum. A low DA concentration results in Parkinson's disease. Since DA and AA

have similar oxidation potentials at most solid electrodes, it is challenging to differentiate them because of their overlapping signals. Our N-doped SWCNTs with high electrochemical activity and conductivity may promote the electron-transfer reactions of DA. We fabricated DA and AA sensors using the N-doped SWCNTs/GC and un-doped SWCNTs/GC to evaluate their sensitivity and selectivity for DA and AA detection. Figure 4c shows CVs of DA and AA in a PBS buffer solution for the N-doped SWCNTs. It can be seen that the oxidation potential difference between DA and AA is about 0.53 V, which is higher than in previous reports.<sup>36-40</sup> Thus, it is much easier for the N-doped SWCNT-based biosensor to discriminate DA from AA. Furthermore, the oxidation peak currents of DA are intense while those of AA are very weak for both the pure solutions and mixed DA and AA (Figure 4d and Figure S4). Compared with pure DA (Figure 4e and Figure S5), the presence of AA in solution has almost no effect on the oxidation potentials of DA. In addition, the peak currents in both the anode and cathode are linearly proportional to the DA concentration in a given range (Figure 5f), indicating that the N-doped SWCNT-based sensor can detect DA quantitatively. The slope of the linear curve in the anode for the N-doped SWCNTs is about 2.5 times that for the un-doped SWCNTs. These results confirm that N-doped SWCNTs are a desirable candidate for use in DA detection sensors.

## Conclusions

Metal-free N-doped SWCNTs were prepared by using SiO<sub>x</sub> as catalyst and ethylenediamine as the source for both carbon and nitrogen. The N-doped SWCNTs have a mean diameter of 1.1 nm and a narrow diameter distribution range. Multi-wavelength laser Raman spectra indicate that the product is enriched with m-SWCNTs when nitrogen is introduced. The surface electrical

resistance of the N-doped SWCNTs remains almost unchanged over a wide temperature range of 20-295 K, confirming that the SWCNTs are metallic. The incorporation of nitrogen may change the interaction between SWCNTs and catalyst during the nucleation stage and hence lead to the growth of thinner, metallic nanotubes. The N-doped SWCNTs were used as electrodes for ORR and DA detection. Due to their unique characteristics of small and uniform diameter, high nitrogen content and metallic feature, the N-doped SWCNTs show high electrocatalytic activity for ORR and a highly sensitive and selective detection capability for DA.

## Acknowledgements

This work was supported by the Ministry of Science and Technology of China (Grants 2011CB932601) and National Natural Science Foundation of China (Grants 51102242, 51221264, and 51272257).

## Notes and references

Shenyang National Laboratory for Materials Science, Institute of Metal Research, Chinese Academy of Sciences, Shenyang 110016, PR China

<sup>§</sup>These authors are equal major contributors

Corresponding Author: [cliu@imr.ac.cn](mailto:cliu@imr.ac.cn) (C. Liu)

<sup>†</sup>Electronic Supplementary Information (ESI) available: Additional information including Raman spectra, ORR polarization curves, CV curves, etc. See DOI: 10.1039/b000000x/

1. S. J. Tans, A. R. M. Verschueren and C. Dekker, *Nature*, 1998, **393**, 49-52.
2. D.-m. Sun, M. Y. Timmermans, Y. Tian, A. G. Nasibulin, E. I. Kauppinen, S. Kishimoto, T. Mizutani and Y. Ohno, *Nat Nano*, 2011, **6**, 156-161.
3. J. Kong, N. R. Franklin, C. Zhou, M. G. Chapline, S. Peng, K. Cho and H. Dai, *Science*, 2000, **287**, 622-625.
4. D. W. H. Fam, A. Palaniappan, A. I. Y. Tok, B. Liedberg and S. M. Moochhala, *Sensors and Actuators B: Chemical*, 2011, **157**, 1-7.
5. M. S. P. Shaffer and A. H. Windle, *Advanced Materials*, 1999, **11**, 937-941.
6. C. Liu, F. Li, L.-P. Ma and H.-M. Cheng, *Advanced Materials*, 2010, **22**, E28-E62.

7. K. Gong, F. Du, Z. Xia, M. Durstock and L. Dai, *Science*, 2009, **323**, 760-764.
8. H. T. Chung, J. H. Won and P. Zelenay, *Nat Commun*, 2013, **4**, 1922.
9. J. Wang, M. Musameh and Y. Lin, *Journal of the American Chemical Society*, 2003, **125**, 2408-2409.
10. Y. Li, D. Mann, M. Rolandi, W. Kim, A. Ural, S. Hung, A. Javey, J. Cao, D. Wang, E. Yenilmez, Q. Wang, J. F. Gibbons, Y. Nishi and H. Dai, *Nano Letters*, 2004, **4**, 317-321.
11. L. Qu, F. Du and L. Dai, *Nano Letters*, 2008, **8**, 2682-2687.
12. L. Ding, A. Tselev, J. Wang, D. Yuan, H. Chu, T. P. McNicholas, Y. Li and J. Liu, *Nano Letters*, 2009, **9**, 800-805.
13. B. Yu, C. Liu, P.-X. Hou, Y. Tian, S. Li, B. Liu, F. Li, E. I. Kauppinen and H.-M. Cheng, *Journal of the American Chemical Society*, 2011, **133**, 5232-5235.
14. W.-S. Li, P.-X. Hou, C. Liu, D.-M. Sun, J. Yuan, S.-Y. Zhao, L.-C. Yin, H. Cong and H.-M. Cheng, *ACS Nano*, 2013, **7**, 6831-6839.
15. Y. Che, C. Wang, J. Liu, B. Liu, X. Lin, J. Parker, C. Beasley, H. S. P. Wong and C. Zhou, *ACS Nano*, 2012, **6**, 7454-7462.
16. A. R. Harutyunyan, G. Chen, T. M. Paronyan, E. M. Pigos, O. A. Kuznetsov, K. Hewaparakrama, S. M. Kim, D. Zakharov, E. A. Stach and G. U. Sumanasekera, *Science*, 2009, **326**, 116-120.
17. Y. Liu, Z. Jin, J. Wang, R. Cui, H. Sun, F. Peng, L. Wei, Z. Wang, X. Liang, L. Peng and Y. Li, *Advanced Functional Materials*, 2011, **21**, 986-992.
18. T. Thurakitseree, C. Kramberger, P. Zhao, S. Aikawa, S. Harish, S. Chiashi, E. Einarsson and S. Maruyama, *Carbon*, 2012, **50**, 2635-2640.
19. Z. Zhu, H. Jiang, T. Susi, A. G. Nasibulin and E. I. Kauppinen, *Journal of the American Chemical Society*, 2010, **133**, 1224-1227.
20. T. Susi, Z. Zhu, G. Ruiz-Soria, R. Arenal, P. Ayala, A. G. Nasibulin, H. Lin, H. Jiang, O. Stephan, T. Pichler, A. Loiseau and E. I. Kauppinen, *physica status solidi (b)*, 2010, **247**, 2726-2729.
21. T. Susi, A. G. Nasibulin, P. Ayala, Y. Tian, Z. Zhu, H. Jiang, C. Roquelet, D. Garrot, J.-S. Lauret and E. I. Kauppinen, *physica status solidi (b)*, 2009, **246**, 2507-2510.
22. H. R. Barzegar, E. Gracia-Espino, T. Sharifi, F. Nitze and T. Wågberg, *The Journal of Physical Chemistry C*, 2013.
23. B. Liu, W. Ren, L. Gao, S. Li, S. Pei, C. Liu, C. Jiang and H.-M. Cheng, *Journal of the American Chemical Society*, 2009, **131**, 2082-2083.
24. S. Li, C. Liu, P.-X. Hou, D.-M. Sun and H.-M. Cheng, *ACS Nano*, 2012, **6**, 9657-9661.
25. R. Liu, D. Wu, X. Feng and K. Müllen, *Angewandte Chemie*, 2010, **122**, 2619-2623.
26. M. S. Dresselhaus, G. Dresselhaus and A. Jorio, *Annual Review of Materials Research*, 2004, **34**, 247-278.
27. A. Jorio, A. G. Souza Filho, G. Dresselhaus, M. S. Dresselhaus, A. K. Swan, M. S. Ünlü, B. B. Goldberg, M. A. Pimenta, J. H. Hafner, C. M. Lieber and R. Saito, *Physical Review B*, 2002, **65**, 155412.
28. E. Iyyamperumal, S. Wang and L. Dai, *ACS Nano*, 2012, **6**, 5259-5265.
29. T. Thurakitseree, C. Kramberger, A. Kumamoto, S. Chiashi, E. Einarsson and S. Maruyama, *ACS Nano*, 2013, **7**, 2205-2211.
30. M. Zhao, Y. Xia, J. P. Lewis and R. Zhang, *Journal of Applied Physics*, 2003, **94**, 2398-2402.
31. F. Villalpando-Paez, A. Zamudio, A. L. Elias, H. Son, E. B. Barros, S. G. Chou, Y. A. Kim, H. Muramatsu, T. Hayashi, J. Kong, H. Terrones, G. Dresselhaus, M. Endo, M. Terrones and M. S. Dresselhaus, *Chemical Physics Letters*, 2006, **424**, 345-352.
32. K. Yanagi, H. Udoguchi, S. Sagitani, Y. Oshima, T. Takenobu, H. Kataura, T. Ishida, K. Matsuda and Y. Maniwa, *ACS Nano*, 2010, **4**, 4027-4032.
33. D. Yu, Q. Zhang and L. Dai, *Journal of the American Chemical Society*, 2010, **132**, 15127-15129.
34. Z. Mo, S. Liao, Y. Zheng and Z. Fu, *Carbon*, 2012, **50**, 2620-2627.
35. K. Balasubramanian and M. Burghard, *Anal Bioanal Chem*, 2006, **385**, 452-468.
36. Z. Wang, J. Liu, Q. Liang, Y. Wang and G. Luo, *Analyst*, 2002, **127**, 653-658.
37. Y. Zhao, Y. Gao, D. Zhan, H. Liu, Q. Zhao, Y. Kou, Y. Shao, M. Li, Q. Zhuang and Z. Zhu, *Talanta*, 2005, **66**, 51-57.
38. R. Cui, X. Wang, G. Zhang and C. Wang, *Sensors and Actuators B: Chemical*, 2012, **161**, 1139-1143.
39. S. Shahrokhian and H. R. Zare-Mehrjardi, *Electrochimica Acta*, 2007, **52**, 6310-6317.
40. M. Zhang, K. Gong, H. Zhang and L. Mao, *Biosensors and Bioelectronics*, 2005, **20**, 1270-1276.